ACS APPLIED MATERIALS & INTERFACES

Research Article

www.acsami.org

Unraveling the Enhanced Photocatalytic Activity and Phototoxicity of ZnO/Metal Hybrid Nanostructures from Generation of Reactive Oxygen Species and Charge Carriers

Weiwei He,[†,‡] Haohao Wu,[‡] Wayne G. Wamer,[‡] Hyun-Kyung Kim,[§] Jiwen Zheng,[¶] Huimin Jia,[†] Zhi Zheng,[†] and Jun-Jie Yin*[,‡]

[†]Key Laboratory of Micro-Nano Materials for Energy Storage and Conversion of Henan Province, Institute of Surface Micro and Nano Materials, Xuchang University, Xuchang, Henan 461000, P. R. China

[‡]Center for Food Safety and Applied Nutrition, U.S. Food and Drug Administration, College Park, Maryland 20740, United States

[§]Ministry of Food and Drug Safety, Osong Health Technology Administration Complex, Cheongju, Chungcheongbuk-do 363-700, Republic of Korea

[¶]Division of Chemistry and Materials Science, Office of Science and Engineering Laboratories, Center for Devices and Radiological Health, U.S. Food and Drug Administration, Silver Spring, Maryland 20993, United States

Supporting Information

ABSTRACT: An effective way for promoting photocatalytic activity of a semiconductor is deposition of noble metal nanoparticles (NPs) onto it. In this paper, we deposited Ag and Pd onto ZnO NPs to form ZnO/Ag and ZnO/Pd hybrid nanostructures. It was found that both Ag and Pd nanocomponents can greatly enhance the photocatalytic activity and phototoxicity of ZnO toward human skin cells. Using electron spin resonance spectroscopy with spin trapping and spin labeling techniques, we observed that either deposition of Ag or Pd resulted in a significant increase in photogenerated electrons and holes and production of reactive oxygen species including hydroxyl radicals, superoxide, and singlet oxygen. We compared the enhancing effects of Ag and Pd and found that Pd is more effective than Ag in promoting the generation of hydroxyl radicals and holes and the photocatalytic activity of ZnO. Conversely, Ag is more effective than Pd in enhancing electron transfer and the generation of superoxide and singlet oxygen. The mechanism underlying the differences in the effects of Ag and Pd may be related to differences in Fermi levels for Ag and Pd and band bending accompanied by effects on Schottky barriers. The results of these studies provide information valuable for designing hybrid nanomaterials having photocatalytic and photobiological activities useful for applications such as water purification and formulation of antibacterial products.

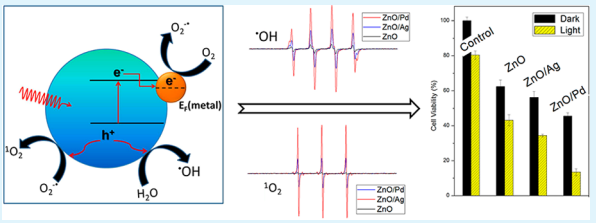

KEYWORDS: *ZnO/Ag, ZnO/Pd, reactive oxygen species, phototoxicity, photocatalytic, ESR*

INTRODUCTION

Metal oxide nanostructures with unique electronic properties and excellent photoactivity have received a great deal of interest. The photocatalytic activity of many metal oxides makes them potentially useful for many applications such as environmental remediation and biomedical use.[1−4] The physicochemical properties and photoactivity of metal oxide nanostructures are strongly dependent on their size,[5,6] shape,[5,6] structures, and surface states.[5,7] The photophysical and photochemical activities of metal oxides have been attributed to photogenerated reactive intermediates whose formation is determined by the energy band gap.[1,2,8] In general, absorption of light having energy equivalent to the band gap of a semiconductor results in charge separation and creation of electron (e^-)/hole (h^+) pairs. The resulting electrons in the conduction band and the holes in valence band show strong reducing and oxidizing power, respectively, and their reducing or oxidizing power is determined by their band edge energy level.[8] Consequently, photogenerated electrons and holes, having sufficient energy, can react with surrounding oxygen containing species such as molecular oxygen, water, or hydroxyl ions to form various reactive oxygen species (ROS) including superoxide, singlet oxygen, and hydroxyl radicals. Currently, both the photocatalytic and photobiological activities of metal oxides are thought to result from photogenerated charge carriers and ROS.

This mechanism suggests two ways to tune the photocatalytic or photobiological activity of metal oxides: (1) tuning the band structure to adjust the reactivity of photogenerated holes and electrons, e.g., doping with other elements,[9] and (2)

Received: July 2, 2014
Accepted: August 12, 2014
Published: August 12, 2014

enhancing the separation efficiency of electron/hole pairs via forming hybrid nanostructures with metal, carbon, or other nanocomponents. For example, combining ZnO or TiO_2 with a noble metal (e.g., Au, Ag, Pt, or Pd) has been demonstrated to result in hybrid nanomaterials with enhanced transport of photogenerated electrons and improved catalytic activity.[10,11] In fact, both a change in the band structure and an increase in separation efficiency will lead to a change in generation of ROS, since generation of ROS is wholly dependent on photogeneration of electrons and holes. A great effort has been made by investigators to develop metal oxides with enhanced photoactivity. However, fewer investigators have studied the mechanism underlying enhanced photoactivity. This knowledge gap limits our understanding of the role of charge carriers and ROS in the photochemical and photobiological reactions of semiconductor nanostructures and our ability to rationally design new photoactive metal oxide nanostructures.

Recently, we have developed an effective method using electron spin resonance spectroscopy coupled with spin trapping and spin labeling techniques to study the charge carriers and ROS generated in the presence of nanomaterials.[12−15] We have found that deposition of Au on ZnO greatly enhanced the photocatalytic and antibacterial activities, which was correlated with enhanced generation of charge carriers and 3 kinds of ROS, superoxide, hydroxyl radicals, and singlet oxygen.[12] We observed that this enhanced effect of Au was mainly attributed to its Fermi level, which being lower than the Fermi level of ZnO, allowed electron transfer from ZnO to Au (Scheme 1). Nel and co-workers have also recently found that

Scheme 1. Schematic Showing How Metals Enhance Electron Transfer and the Photogeneration of ROS

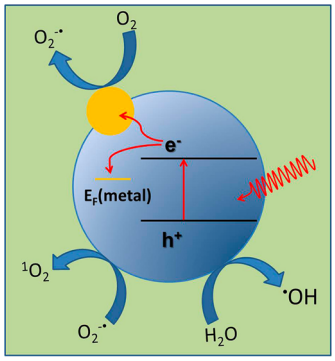

the relative Fermi levels of Co_3O_4 and the dopant, PdO, largely determined the biological effects of doped Co_3O_4.[16] These results demonstrate the importance of understanding the mechanisms through which hybrid nanostructures possess enhanced photocatalytic and photobiological activities. This paper describes a mechanistic investigation of how metals with different Fermi levels affect the photoactivity and generation of ROS for ZnO nanostructures.

In this work, we have used our versatile electron spin resonance technique to compare the enhancing effect of Ag and Pd nanoparticles (NPs) on both the separation efficiency of charge carriers and the generation of ROS in ZnO hybrid nanostructures. Zinc oxide was selected as a representative metal oxide because of its widespread commercial use. We compared not only the abilities of Ag and Pd in enhancing the generation of hydroxyl radicals, superoxide, singlet oxygen, electrons, and holes by photoexcited ZnO but also the enhancing effect on the photocatalytic degradation and photoinduced cellular toxicity of ZnO nanostructures. In addition, the mechanism leading to the difference between the effects of Ag and Pd and the correlation between photocatalytic activity/phototoxicity and the ROS production were investigated.

EXPERIMENTAL SECTION

Chemical and Materials. Potassium tetrachloropalladate (II) (K_2PdCl_4), silver nitrate ($AgNO_3$), methylene blue (MB), salicylic acid, NaN_3, superoxide dismutase (SOD), 2,2,6,6-tetramethyl-4-piperidon (4-oxo-TEMP), and standard buffer solutions were purchased from Sigma-Aldrich Chemical Co. (St. Louis, MO). An aqueous dispersion of zinc oxide nanoparticles (20 wt %, 30−40 nm) was purchased from US Research Nanomaterials, Inc. (Houston, TX). The spin-trap 5-tert-butoxycarbonyl 5-methyl-1-pyrroline *N*-oxide (BMPO) was purchased from Applied Bioanalytical Laboratories (Sarasota, FL). 1-Hydroxy-3-carboxy-2,2,5,5-tetramethylpyrrolidine (CPH) and 2,2,6,6-tetramethylpiperidine-1-oxyl (TEMPO) were purchased from Alexis, Enzo Life Sciences, Inc. (NY, USA). Milli-Q water (18 MΩ cm) was used for preparation of all solutions.

Synthesis of ZnO/Ag and ZnO/Pd Hybrid Nanostructures. ZnO/Ag and ZnO/Pd hybrid nanostructures were prepared using a similar method to that used for preparation of ZnO/Au nanostructures.[12] In a typical synthesis, 2 mL of 5.0 mg/mL ZnO suspension was mixed with 29 μL of 0.1 M $AgNO_3$ or K_2PdCl_4 aqueous solution in a quartz tube and sealed. The molar percentage of Ag or Pd to ZnO in this representative reaction was 2%. The above solutions were sonicated for 2 min, and then irradiated for 15 min for ZnO/Ag and 45 min for ZnO/Pd with a 450 W xenon lamp. A clearly evident color change from white to dark gray indicated the formation of ZnO/Ag or ZnO/Pd hybrid nanostructures. We refer to the product of this reaction as ZnO/Ag2% or ZnO/Pd2%. The precipitate was collected by centrifugation, washed three times with water, and diluted to 1.0 mL with water for further experiments.

Characterization. Transmission electron microscopy (TEM) images were captured on a JEM 2100 FEG (JEOL) transmission electron microscope (accelerating voltage of 200 kV) located at the NanoCenter, University of Maryland, College Park, MD. Energy-dispersive X-ray analysis (EDX) was conducted using the same microscope. The samples for TEM analysis were prepared by adding drops of the dispersed colloidal solutions onto standard holey carbon-coated copper grids, which were then air-dried at room temperature. The crystal structure of synthesized products was characterized by X-ray diffraction (XRD, Bruker D8 Advance diffractometer) using monochromatized Cu Kα radiation (λ = 1.5418 Å). UV−vis absorption spectra were obtained using a Varian Cary 300 spectrophotometer.

The photocatalytic activities of ZnO, ZnO/Ag, and ZnO/Pd hybrid nanostructures were evaluated by measuring the degradation of methylene blue (MB) and salicylic acid (SA) in aqueous solutions. 0.1 mg/mL of ZnO, ZnO/Ag, or ZnO/Pd photocatalyst was dispersed in a 10 mL aqueous solution containing 0.01 mg/mL MB or 0.5 mM SA. The solution was continuously stirred in the dark for 30 min to establish an adsorption−desorption equilibrium between the photocatalyst and substrate. Then, the suspension, with constant stirring, was irradiated using an 800 W xenon lamp filtered to deliver simulated sunlight. At selected time intervals, aliquots of suspension were collected and centrifuged. The residual concentration of the MB or SA in the supernatant was monitored using a Varian Cary 300 spectrometer.

Cell Culture. Human skin fibroblasts (ATCC CRL-1634) were obtained from the American Type Culture Collection (Manassas, VA). Cells were cultured in Dulbecco's modified Eagle's medium, without phenol red, containing 10% fetal bovine serum, 50 μg/mL gentamicin, 4.5 mg/mL glucose, and 4 mM L-glutamine. All reagents used for cell culture were obtained from Invitrogen Corp., Carlsbad, CA. Cultures were incubated at 37 °C in a humidified atmosphere containing 5% CO_2.

In Vitro Assay for Cytotoxicity and Photocytotoxicity. Fibroblasts were seeded into 24-well plates (~5 × 10^4 cells per well) and incubated overnight. The fibroblasts were then incubated for 24 h with media containing 10 μg/mL nanomaterials. Four replicate wells were used for each treatment. Stock solutions of the nanomaterials were prepared by dispersing the nanomaterials in deionized water using a 10 s ultrasonic burst (Vibra-Cell VC250B sonicator, Sonics & Materials Inc., Danbury. CT). The stock solution was then heated for 10 min at l00 °C to minimize microbial contamination. Working solutions for treating fibroblasts were prepared by appropriately diluting stock solutions with media.

Following the 24 h incubation in media containing the nanomaterials, fibroblasts were washed twice with phosphate-buffered saline (PBS, pH 7.4). Fibroblasts were then irradiated through freshly added PBS with 10 J/cm^2 UVA radiation (320−400 nm) combined with 45 J/cm^2 visible light (400−800 nm). The source of UVA radiation and visible light was a 250-W HITLite metal halide bulb (BLV Licht-and-Vakuumreenik GmbH, Sreinhöring, Germany) filtered through glass. The emission spectrum of the light source was measured using an OL 754 UV−visible spectroradiometer (Optronic Laboratories Inc., Orlando, FL). The spectral irradiance of the light source was found to be typically 6.3 × 10^{-3} W/cm^2 UVA radiation and 2.8 × 10^{-2} W/cm^2 visible light. The emission of UVB radiation (280 nm-320 nm) from the light source was negligible (i.e., 11 × 10^{-7} W/cm^2). All irradiations were performed at 25° ± 3 °C and lasted approximately 10 min for simultaneous delivery of 10 J/cm^2 UVA radiation and 45 J/cm^2 visible light. To compensate for any inhomogeneity in the field of illumination, uncovered samples were placed on a platform that rotated at 0.5 rpm during irradiation. Sham-irradiated (i.e., dark control) samples were maintained at 25° ± 3 °C in the dark. After irradiation, fresh media was added and the plates were incubated for 2−3 days to allow cell growth. Following the incubation, wells were washed twice with PBS, and 0.2 mL of 40 mM sodium *N*-lauroylsarcosine was added to each well. At least 15 min was then allowed for cell lysis. Protein concentration in the lysate was determined according to Lowry's method using reagents in the Sigma Chemical Co. protein assay kit (catalogue No.P5656).[17] The percentage viability for cells was calculated using the following formula: [μg protein in treated well/μg protein in control well] × 100.

Electron Spin Resonance Spectroscopy. All the electron spin resonance (ESR) measurements were carried out using a Bruker EMX ESR spectrometer (Billerica, MA) at room temperature. A solar simulator consisting of a 450 W xenon lamp filtered to provide simulated sunlight was used in ESR studies. Fifty microliter aliquots of control or sample solutions were put into quartz capillary tubes with internal diameters of 0.9 mm and sealed. The capillary tubes were inserted in the ESR cavity, and the spectra were recorded during irradiation at selected times. Other settings were as follows: 1 G field modulation, 100 G scan range, and 20 mW microwave power for detection of spin adducts using spin traps and 0.04 G field modulation, 5 G scan range.

The spin trap BMPO was used to verify the formation of superoxide (·OOH) and hydroxyl radicals (·OH). 4-oxo-TEMP was used to demonstrate the generation of singlet oxygen. CPH and TEMPO were used as spin probes for studying the holes and electrons generated during photoexcitation of ZnO hybrid nanostructures. In these experiments, the intensity of the ESR signal was measured as the peak-to-peak height of the second line of ESR spectrum. ESR spectra were recorded from the sample mixture, containing spin probes (BMPO, 4-oxo-TEMP, CPH, or TEMPO) and nanoparticles (ZnO, ZnO/Ag, or ZnO/Pd), after exposure to simulated sunlight for selected times. For comparison, the controls either without catalysts or without irradiation were also recorded. The final concentration of each component is described in each figure caption.

RESULTS AND DISCUSSION

Formation of ZnO/Ag and ZnO/Pd Hybrid Nanostructures. ZnO/Ag and ZnO/Pd hybrid nanostructures were synthesized by irradiating a mixture containing ZnO nanoparticles and $AgNO_3$ (Ag^+) or $PdCl_4^{2-}$ (Pd^{2+}). After photoreduction of Ag^+ or Pd^{2+} in the presence of ZnO NPs, the originally white suspension changed to dark gray indicating formation of ZnO/Ag and ZnO/Pd hybrid nanostructures. Figure 1 displays the TEM images of prepared ZnO/Ag and

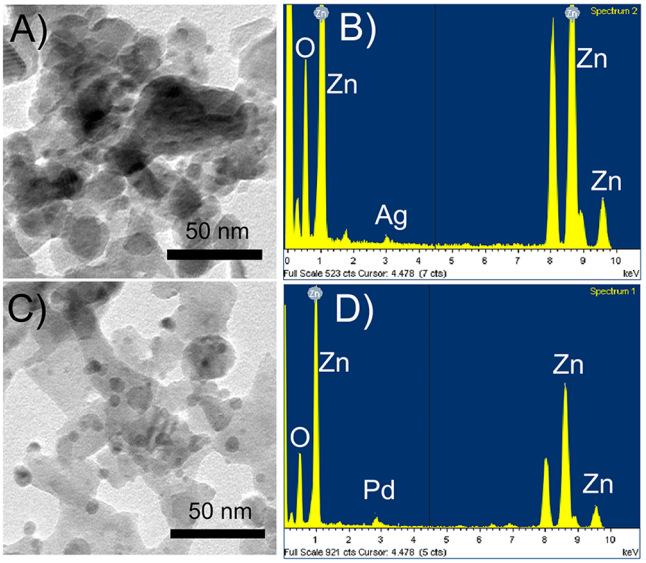

Figure 1. TEM images of prepared ZnO/Ag (A) and ZnO/Pd (C) hybrid nanostructures and energy-dispersive X-ray spectroscopic analysis of ZnO/Ag (B) and ZnO/Pd (D) hybrid nanostructures.

ZnO/Pd hybrid nanostructures from pure ZnO NPs. The dark dots distributed on the surface of ZnO refer to Ag (Figure 1A) or Pd nanoparticles (Figure 1C). We calculated the average size of Ag and Pd dots to be 5.2 ± 1.2 and 6.5 ± 0.9 nm, respectively. Energy-dispersive X-ray (EDX) analysis confirms the coexistence of Ag and Zn in the ZnO/Ag hybrid nanostructures (Figure 1B) and Pd and Zn in the ZnO/Pd hybrid nanostructures (Figure 1D). The atomic ratio Ag/Zn measured from EDX is 1.8% in ZnO/Ag sample, and the Pd/Zn ratio is measured to be 2.3%. These results are consistent with the calculated stoichiometric ratio of Ag/ZnO and Pd/ZnO with molar ratio of 2% and suggests a complete conversion of Ag^{2+} (Pd^{2+}) to Ag (Pd). The XRD pattern further supports the formation of ZnO/Ag and ZnO/Pd hybrid structures (Figure 2). The diffraction peaks for pure ZnO samples can be indexed to the hexagonal phase of the zincite structure (JCPDS NO. 1-1136), with no additional impurity peaks. After deposition of Ag at a reactant molar ratio of 2% (Ag/ZnO), a characteristic peak of Ag (111) appeared indicating the formation of crystalline Ag. Also, the accompanying diffraction peak of Pd (111) in the ZnO/Pd sample indicated the formation of crystalline Pd. The deposition of Ag and Pd onto ZnO will influence the optical response of ZnO (Figure S1, Supporting Information). At short wavelengths, we observed stronger absorption intensity below 350 nm for ZnO/Pd and ZnO/Ag than for pure ZnO NPs. At longer wavelengths, above 400 nm, ZnO/Pd had a similar absorption to ZnO but ZnO/Ag exhibited a higher absorption band, which may be attributed to the weak surface plasmon resonance (SPR) effect of Ag nanodots on the ZnO surface. The band gap energy (E_g) was calculated on the basis of the absorption spectra using the formula, $\alpha h\nu = A(h\nu - E_g)^{1/2}$, where α is the absorption coefficient, A is a constant, and $h\nu$ is

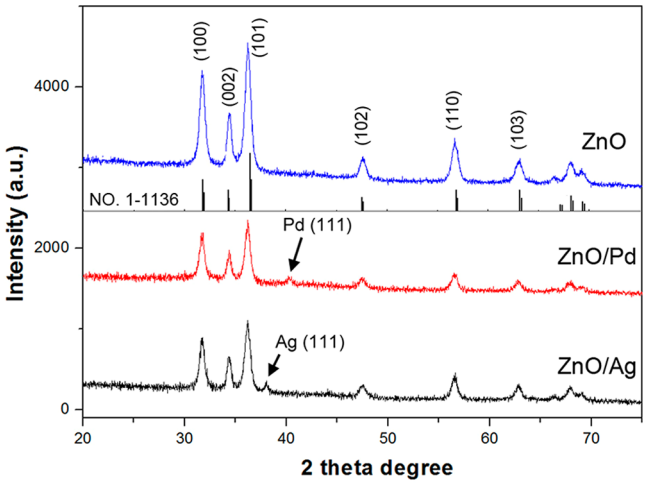

Figure 2. XRD patterns of ZnO, ZnO/Pd, and ZnO/Ag nanostructures.

the photon energy. Compared with ZnO, deposition of Pd led to a 7% increase in the band gap, while deposition of Ag resulted in a slight increase of about 2% (Figure S1 inset, Supporting Information).

Enhanced Photocatalytic Activity and Photoinduced Cellular Toxicity of ZnO/Ag and ZnO/Pd Hybrid NPs. The photodegradation of two representative pollutants, organic dye methylene blue (MB) and colorless pollutant salicylic acid (SA), was determined to evaluate the photocatalytic activity of ZnO, ZnO/Ag, and ZnO/Pd hybrid nanostructures (Figure 3). The control experiments show MB and SA are resistant to degradation during irradiation without photocatalyst. Pure ZnO nanoparticles show considerable catalytic ability for both the degradation of MB and SA under simulated sunlight. For Ag and Pd deposited ZnO at molar ratio of ~2%, the degradation of both MB and SA was significantly enhanced. In the degradation of MB, ZnO/Pd has a photocatalytic activity (degradation degree) about 3.5 times higher than ZnO and 2 times higher than ZnO/Ag after a 20 min irradiation. For the degradation of SA, ZnO/Pd shows the photocatalytic activity about 4 times higher than ZnO and 2 times higher than ZnO/Ag after 180 min irradiation. The degradation of MB and SA in the presence of ZnO, ZnO/Ag, and ZnO/Pd was found to be a pseudo-first order kinetic process (Figure 3B,D). The MB degradation rate constants for ZnO, ZnO/Ag, and ZnO/Pd were calculated to be 0.015, 0.025, and 0.097 min^{-1}, respectively. The SA degradation rate constants of ZnO, ZnO/Ag, and ZnO/Pd were calculated to be 0.00067, 0.00169, and 0.0037 min^{-1}. These results verify that deposition of Ag and Pd onto ZnO significantly enhances the photocatalytic activity of ZnO. This enhancement of photocatalytic activity may be correlated with their enhanced effect on the generation of ROS that will be discussed.

Apart from photocatalytic degradation of organic molecules, ZnO can also cause photobiological effects due to photogenerated ROS. To examine whether Ag and Pd can enhance

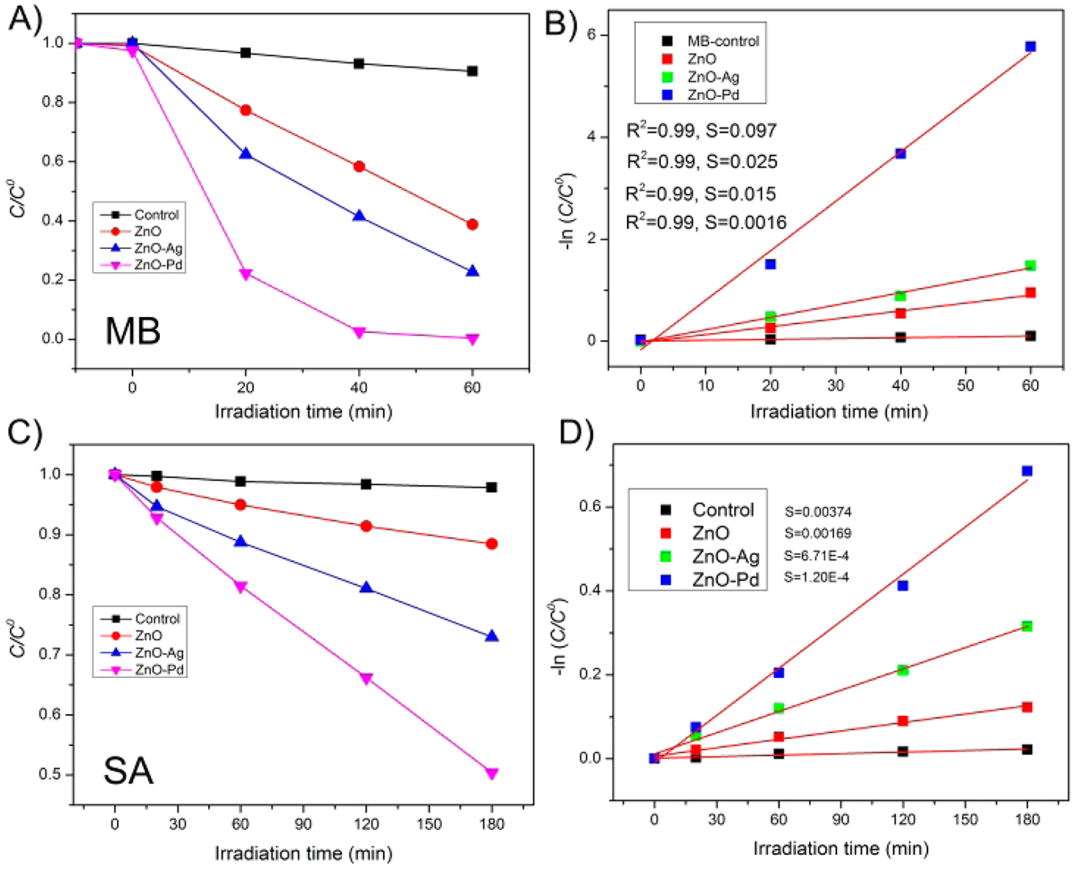

Figure 3. Photocatalytic activity of ZnO, ZnO/Ag, and ZnO/Pd NPs for the degradation of MB and salicylic acid under simulated sunlight. The figure shows the concentration change of MB (A) and SA (C) and $-\ln(C/C^0)$ as a function of irradiation time during the degradation of MB (B) and SA (D). The concentration of photocatalysts are fixed at 0.1 mg/mL.

the photobiological activity of ZnO, we compared the photoinduced cellular toxicity of ZnO nanoparticles with that of ZnO/Ag and ZnO/Pd hybrid nanostructures using human skin fibroblasts (Figure 4). Exposure to light alone slightly

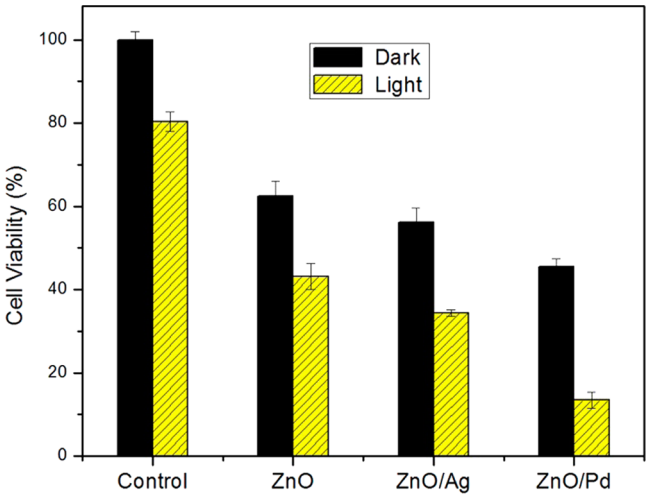

Figure 4. Effect of ZnO, ZnO/Ag, and ZnO/Pd nanoparticles on viability of human skin fibroblasts before and after irradiation with light (λ>320 nm) for 10 min. Cells were treated with NPs at a concentration of 10 μg/mL. Data shown are mean values from 3 independent experiments (n = 3).

reduced the survival of fibroblasts. This may be caused by the UVA component emitted by the light source. Exposure to 10 μg/mL ZnO, ZnO/Ag, or ZnO/Pd NPs prior to and during irradiation resulted in a considerable reduction in cellular viability. Also, we found that ZnO/Ag and ZnO/Pd NPs were more photocytotoxic than ZnO NPs. It has been reported that ZnO NPs, even without irradiation, can cause cellular toxicity. This toxicity has been attributed to Zn^{2+} released from ZnO NPs or physical interaction between cellular structures and ZnO NPs.[18,19] Ag NPs have been recognized as antibacterial agents and their mechanism for inducing toxicity has been, and continues to be, intensively investigated.[20] Recent reports have also proposed that Pd NPs could inhibit the growth of bacterial cultures and induce cytotoxicity via triggering caspase-dependent apoptosis or otherwise modulating intracellular chemistry.[21−23] Therefore, ZnO combined with Pd or Ag nanodots is expected to induce higher toxicity than pure ZnO at the same dosage of ZnO, because of the additional toxicity of Pd and Ag NPs alone. When fibroblasts were exposed to both NPs and light, cellular viability was decreased significantly to 45%, 34%, and 13% by ZnO, ZnO/Ag, and ZnO/Pd NPs, respectively, from 62%, 56%, and 47% before irradiation. Comparing the results before and after irradiation, it is clear that these NPs are phototoxic to human skin fibroblasts and the phototoxicity order is ZnO/Pd > ZnO/Ag >ZnO. This relative order in phototoxicity is the same as the relative order in photocatalytic activity discussed earlier.

A number of investigators have reported mechanistic links between the photocatalytic activity and phototoxicity of metal oxide nanostructures and photogenerated ROS.[24,25] In a similar manner, we have investigated the link between enhancement of the photoactivity of ZnO by Ag or Pd and generation of ROS.

Enhancing Effect of Ag and Pd on the Generation of ROS and Charge Carriers for ZnO Hybrid Nanostructures. It is well-known that photons with energy similar to the band gap energy will be absorbed by ZnO and will generate hole/electron pairs and consequently reactive oxygen species.[26] Electron spin resonance spectroscopy coupled with spin trapping and spin labeling techniques has been demonstrated to be an effective way to obtain specific information on the generation of ROS and charge carriers during photocatalytic processes for nanomaterials. By selection of appropriate spin traps or labels, radicals and charge carriers can be definitively identified and their relative amounts compared.[12] For example, BMPO is a typical spin trap for hydroxyl radical and superoxide; 4-oxo-TEMP is valuable for detection of singlet oxygen, and 2,2,6,6-tetramethylpiperidine-1-oxyl (TEMPO) and 1-hydroxy-3-carboxy-2,2,5,5-tetramethylpyrrolidine (CPH) may be used for characterization of electrons and holes, respectively. Here, we employed this ESR method to investigate the enhancing effect of Ag and Pd on ZnO NPs for generating ROS and charge carriers during irradiation.

Figure 5 shows the ESR spectra obtained from solutions containing various spin probes and ZnO, or ZnO/Ag, and ZnO/Pd hybrid nanostructures before and during irradiation with simulated sunlight. No, or a very weak, ESR signal was observed for control samples (unirradiated samples or samples without NPs) when BMPO, 4-oxo-TEMP, or CPH were used. BMPO was chosen to verify the generation of hydroxyl radicals and superoxide induced by ZnO, ZnO/Ag, or ZnO/Pd. When irradiated with simulated solar light for 3 min in the presence of ZnO, we clearly observed a four-line spectrum with hyperfine splitting parameters of a_N = 13.56, a_H^β = 12.30, and a_H^γ = 0.66. This is the characteristic spectrum for the spin adduct formed between BMPO and the hydroxyl radical, BMPO/·OH.[27] This signal produced from ZnO was attributed to both the hydroxyl radicals and superoxide and was confirmed by studying the effects of scavenging with DMSO and SOD as we previously described.[12,26] When ZnO/Ag or ZnO/Pd hybrid nanostructures were added, the ESR signal for BMPO/·OH increased significantly (Figure 5A). Using the same amount of nanomaterial and irradiation time, the ESR signal intensity generated with ZnO/Pd is calculated as about 2 times as the signal with ZnO/Ag and about 8 times as the signal from pure ZnO. These results indicate that deposition of Ag or Pd onto ZnO significantly enhances photogeneration of hydroxyl radicals and superoxide and that enhancement by Pd is greater than by Ag. Since the detected ESR signal from BMPO is a mixture of BMPO/·OOH and BMPO/·OH, it is necessary to determine the contribution of each radical to the total signal. To determine this, 1.0 U/mL SOD, an amount in excess of that needed to scavenge superoxide in this system, was added to reduce the superoxide and calculate its contribution for each of the nanoparticles (Figure S2, Supporting Information). When SOD was added, the signal intensity decreased by about 44%, 65%, and 35% for ZnO, ZnO/Ag, and ZnO/Pd NPs, respectively. SOD is a specific scavenger for superoxide and has no effect on hydroxyl radicals. These results further indicated that, while hydroxyl radical and superoxide contributed to ESR signal when BMPO was used, superoxide dominated for irradiated ZnO/Ag while hydroxyl radicals dominated for ZnO/Pd in comparison with pure ZnO. In reactions photocatalyzed by ZnO NPs, the production of ROS is related to the photogenerated hole−electron pairs. Dissolved oxygen accepts electrons which have been photoexcited into the conduction band of ZnO. This enables the generation of superoxide. The holes, formed during photoexcitation of ZnO, react with H_2O or OH^- and result in the production of

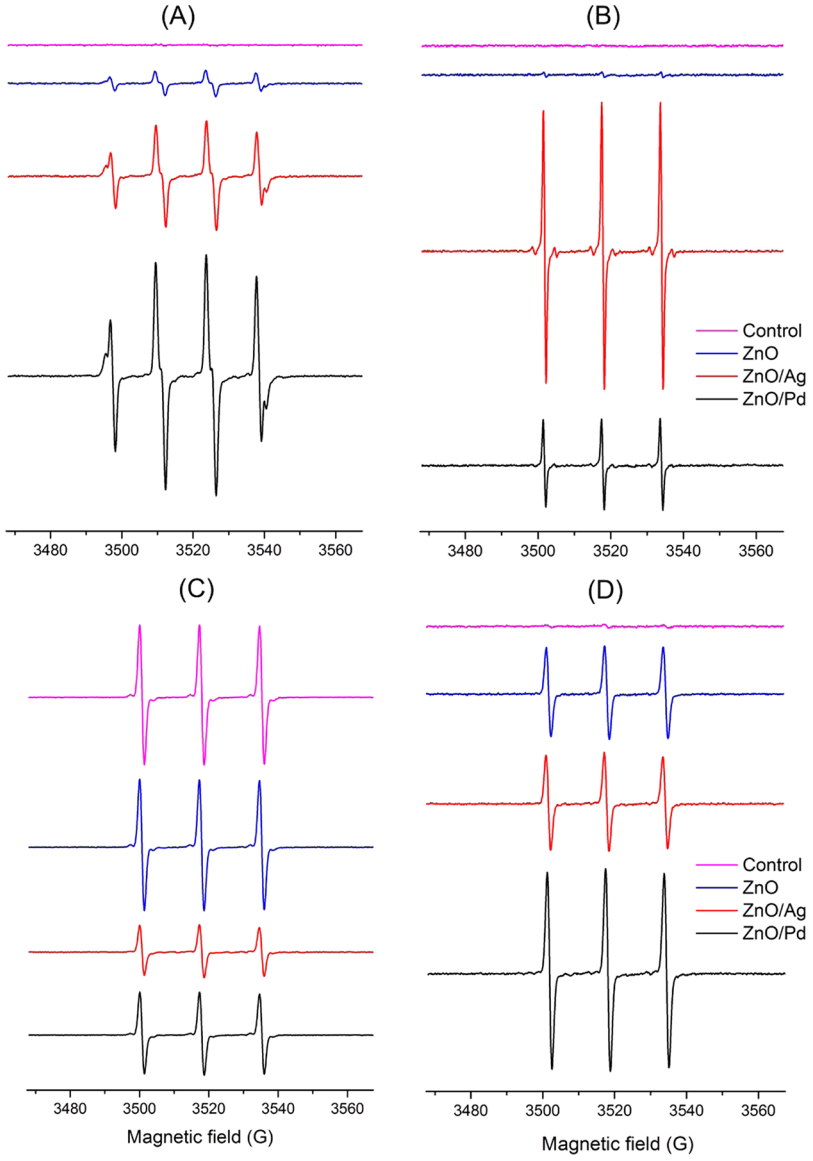

Figure 5. Enhancement effect of Ag and Pd on ZnO nanostructures for generation of ROS and holes/electrons under simulated sunlight. ESR spectra obtained from samples containing 0.1 mg/mL nanostructures (ZnO, ZnO/Ag2%, or ZnO/Pd2%) and spin probes of 25 mM BMPO (A), 0.5 mM 4-Oxo-TEMP (B), 0.02 mM TEMPO (C), or 0.02 mM CPH (D), respectively. The control represents the sample containing spin probe alone under simulated sunlight or the sample containing spin probe and catalysts before exposure to simulated sunlight. The ESR spectra were recorded after 3 min (A, B, and D) or 8 min (C) of irradiation with simulated sunlight.

hydroxyl radicals. These results suggest that the deposition of Ag and Pd may change the transport behavior and reactivity of electron−holes pairs generated in photoexcited ZnO.

In addition to the hydroxyl radical and superoxide, photoexcitation of ZnO NPs can also result in the generation of singlet oxygen via electron transfer from superoxide to holes.[12] 4-oxo-TEMP, a spin trap for singlet oxygen, was used to investigate the enhancing effect of Ag and Pd on singlet oxygen generation (Figure 5B). Compared with control, the triplet spectrum was detected during irradiation of either ZnO or ZnO/Ag and ZnO/Pd hybrid nanostructures (Figure 5B). This ESR spectrum is characteristic for the product formed through the reaction between 4-oxo-TEMP and singlet oxygen. Either 10 mM NaN_3 or 1 U/mL SOD can completely inhibit the ESR signal of 4-oxo-TEMP generated from irradiated ZnO/Ag or ZnO/Pd NPs, further confirming the production of singlet oxygen through a mechanism involving superoxide (Figure S3, Supporting Information). The deposition of Ag or Pd onto ZnO clearly enhanced the generation of singlet oxygen, as seen by the increase in the ESR signal (Figure 5B). We have calculated that the ESR signal intensity generated from photoexcited ZnO/Pd is about 10 times as high as signal from ZnO. It is noteworthy that the signal intensity in the presence of ZnO/Ag is more than 30 times higher than the signal from samples containing ZnO. These results indicate that hybrid nanostructures containing Ag are more efficient than those containing Pd in promoting photogeneration of singlet oxygen. This is consistent with the observation that more superoxide was generated for ZnO/Ag than for ZnO/Pd since superoxide is involved in production of singlet oxygen.

2,2,6,6-Tetramethylpiperidine-1-oxyl (TEMPO) and CPH were used for characterizing the electrons and holes, respectively, generated during photoexcitation of ZnO, ZnO/Ag, and ZnO/Pd (Figure 5C,D). TEMPO, having a stable ESR

signal with a triplet spectrum, does not react with holes and ROS or with unirradiated ZnO nanoparticles. However, it can be reduced by photogenerated electrons to give a hydroxyl amine (TEMPOH) which lacks an ESR signal. Therefore, generation of photoinduced electrons and their reactivity can be easily monitored by observing changes in the ESR spectrum of TEMPO. No signal change was observed for TEMPO itself without catalysts even during irradiation. When TEMPO was irradiated in the presence of ZnO, we observed a slight decrease of TEMPO signal intensity. For ZnO/Ag and ZnO/Pd hybrid nanostructures, an evident reduction of TEMPO signal was observed. Within 8 min of irradiation, about 65% of the signal intensity was reduced during irradiation of samples containing ZnO/Ag, while only 8% reduction was caused by pure ZnO, indicating the photogeneration of electrons for ZnO/Ag was enhanced greatly. Since the consumption of TEMPO is correlated directly with photoinduced electrons, the level of electrons during irradiation of ZnO can be estimated on the basis of the one electron reduction of TEMPO. This is clearly an underestimate of photoinduced electron reactions since targets other than TEMPO may be simultaneously reduced. After 8 min of irradiation, a 50 μL solution containing 0.1 mg/mL ZnO results in approximately 5.0×10^{13} electrons available for photoreduction. However, ZnO/Ag and ZnO/Pd can lead to generation of approximately 4.0×10^{14} and 2.5×10^{14} electrons under 8 min of irradiation, respectively. These results indicate that deposition of Ag or Pd onto ZnO can greatly enhance the reactivity of the photoinduced electrons. CPH can be very slowly oxidized to form nitroxides by dissolved oxygen. CPH is an often-used hole scavenger as it can be oxidized by holes.[28] The oxidation of CPH was used to reflect the photooxidizing activity of catalysts. When CPH is exposed to simulated sunlight in the presence of ZnO or ZnO/Ag or ZnO/Pd, we observe ESR spectra consisting of three-lines with hyperfine splitting constant a_N= 16.2 G. The ESR signal is approximately 2 times greater when irradiating ZnO/Pd compared to ZnO. These results indicate that Pd decorated ZnO will generate holes more effectively during photoexcitation and will be more photocatalytically active than Ag decorated ZnO.

Using ESR spectroscopy, we have compared the effects of Ag and Pd on enhancing generation of electrons, holes, hydroxyl radical, superoxide anion, and singlet oxygen during photoexcitation of ZnO NPs and hybrid nanostructures. Although deposition of Ag or Pd onto ZnO can greatly enhance the generation of all the ROS, electrons, and holes during photoexcitation, Ag and Pd exhibit different behaviors in altering the production of ROS. For example, Ag is more efficient in producing singlet oxygen and Pd is more efficient in generating hydroxyl radicals and holes. By aligning the ESR analysis with photocatalytic activity and phototoxicity, it is plausible to conclude that (1) the enhancement of Pd and Ag on the photoactivity of ZnO correlates closely with their ability in improving charge carrier reactivity and the generation of ROS, and (2) among those photoinduced reactive species, the hydroxyl radicals and highly active holes may dominantly contribute to the enhancing effect of ZnO/Pd hybrid nanostructures on photocatalytic activity and phototoxicity.

Energy Band Structures in ZnO/Ag and ZnO/Pd Determine Their Enhancing Effect in Generation of ROS and Charge Carriers. We have examined the mechanism for formation of ROS during irradiation of ZnO and also verified that metal nanocomponents (e.g., Ag and Pd, Au) can greatly enhance the ROS generation and photocatalytic activity of ZnO. As we pointed out in an earlier publication examining ZnO/Au hybrid nanostructures, the lower Fermi level of Au compared to ZnO results in facilitated electron transfer from the conduction band of ZnO to Au, thus enhancing the separation of charge carriers and generation of ROS.[12] The Fermi levels of Ag ($E_{F,Ag}$) and Pd ($E_{F,Pd}$) are 4.24 and 5.2 eV, respectively. Both of these levels are lower than the conduction band edge of ZnO (4.2 eV). This indicates that both Ag and Pd have the ability to store electrons generated during photoexcitation of ZnO. Ostensibly, Pd should be more effective than Ag in enhancing the separation of charge carriers because of its lower Fermi level. However, this is not entirely consistent with our ESR results for TEMPO reduction and generation of superoxide which showed that ZnO/Ag made more electrons available during irradiation than ZnO/Pd.

In fact, the contact between metal and ZnO, and accompanying band bending, are factors affecting the differences we observed for Ag and Pd in promoting ROS generation. Scheme 2 shows the energy band diagrams of Ag or Pd in contact with ZnO at disequilibrium and equilibrium. When Ag or Pd are in contact with the n-type semiconductor, ZnO, a Schottky contact is formed and the electrons in the conduction band of ZnO will transfer from ZnO to metal due to the lower Fermi levels of Ag and Pd. The electron transfer will continue until the Fermi levels of Ag or Pd ($E_{F,Ag}$ and $E_{F,Pd}$) and ZnO ($E_{F,ZnO}$) are aligned. At equilibrium, the metal Ag or Pd is negatively charged and ZnO is positively charged near their surface. This charge separation will establish a double layer at the Ag/ZnO and Pd/ZnO interface, and a space charge region will be formed with accompanying band bending (Scheme 2). Because $\phi_{m,Ag}$ (4.24 eV, the work function of Ag) < ϕ_{ZnO} (4.65 eV, the work function of ZnO), the energy bands bend downward toward the interface for ZnO/Ag. In contrast, the energy bands bend upward toward the interface for ZnO/Pd since $\phi_{m,Pd}$ (5.2 eV, the work function of Pd) > ϕ_{ZnO}.[29] The different band bending directions between Ag and Pd determined the direction of the intrinsic electric field and

Scheme 2. Energy Band Diagrams for Ag, Pd, and ZnO in Contact before (A) and after (B) Equilibrium[a]

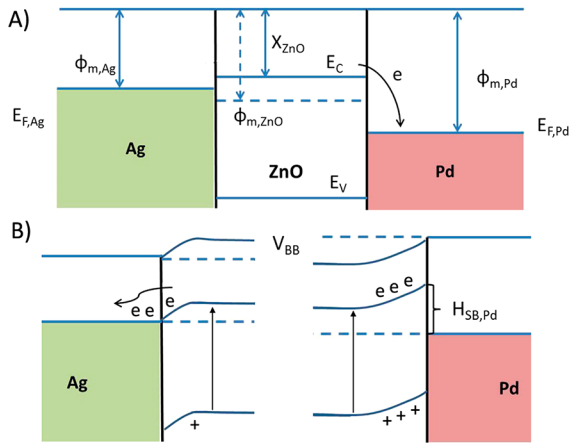

[a] $E_{F,Ag}$ and $E_{F,Pd}$, the Fermi levels of Ag and Pd; E_C, energy of conduction band edge of ZnO; E_V,energy of valence band edge of ZnO; ϕ_m, work function of metal (Ag or Pd); ϕ_{ZnO}, work function of ZnO; X_{ZnO}, electron affinity of ZnO; H_{SB}, Schottky barrier height; V_{BB}, band bending.

polarization electric field in ZnO/Ag and ZnO/Pd. It has been reported that the electrons were accelerated by the polarization electric field in ZnO/Ag but not by ZnO/Pt (the work function of Pt is 5.10 eV).[30] Also, there is a Schottky barrier formed at the ZnO/Pd interface. The Schottky barrier height can be determined to be 1.0 eV by the equation:

$$H_{SB,Pd} = \phi_{m,Pd} - X_{ZnO}$$

where $H_{SB,Pd}$ is the formed Schottky barrier height, and X_{ZnO} is electron affinity of ZnO. According to this analysis, ZnO/Pd may slow the electrons' transfer from ZnO to Pd at equilibrium due to the band bending and Schottky barriers. This interpretation is consistent with the TEMPO data for the ZnO/Ag and ZnO/Pd hybrid nanostructures. This may result in more photogenerated holes accumulated at the interface that exhibit higher oxidizing ability and enhance the formation of hydroxyl radicals. Therefore, ZnO/Pd shows a higher photocatalytic activity and phototoxicity than ZnO/Ag. This also suggests that superoxide and singlet oxygen may play a relatively small role in photoinduced reactions. However, this concept and the possible mechanism we propose for the difference in enhancing behavior of Ag and Pd must be verified through additional studies.

CONCLUSIONS

The ZnO/Ag and ZnO/Pd hybrid nanostructures were synthesized and found to exhibit significant increases in photocatalytic activity, phototoxicity, and generation of ROS and charge carriers. The photocatalytic degradation of pollutant molecules and phototoxicity to human skin cells shared the same trend among the three nanostructures: ZnO/Pd > ZnO/Ag >ZnO. Using ESR spectroscopy with spin trapping and spin labeling techniques, we definitively determined the ROS and charge carriers generated from ZnO, ZnO/Ag, and ZnO/Pd hybrid nanostructures when excited with simulated sunlight. Although both Ag and Pd can enhance the generation of charge carrier and ROS due to their ability in capturing electrons from the conduction band of ZnO, Pd is more effective in enhancing photogeneration of hydroxyl radicals and holes, while Ag is more effective in facilitating photogeneration of electrons, superoxide, and singlet oxygen. This difference in enhancement between Ag and Pd may be attributed to the differences in band bending when the metals are in contact with ZnO and the accompanying Schottky barrier of ZnO/Pd. These results not only demonstrate an effective way to improve photocatalytic and phototoxicity of semiconductors by incorporation of metals but also provide specific information for understanding the mechanisms underlying the photocatalytic and phototoxic properties of semiconductors and hybrid nanostructures.

ASSOCIATED CONTENT

Supporting Information

UV−visible absorption spectra of ZnO, ZnO/Ag, and ZnO/Pd (Figure S1), the effect of SOD on the ESR signal (BMPO as spin trap) generated from photoexcited ZnO, ZnO/Ag, and ZnO/Pd nanostructures (Figure S2), effect of SOD and NaN_3 on the ESR signal of 4-oxo-TEMP generated from ZnO/Ag or ZnO/Pd nanostructures when exposed to simulated sunlight (Figure S3). This material is available free of charge via the Internet at http://pubs.acs.org.

AUTHOR INFORMATION

Corresponding Author

*E-mail: junjie.yin@fda.hhs.gov.

Notes

The authors declare no competing financial interest.

ACKNOWLEDGMENTS

W. He thanks the National Natural Science Foundation of China (Grant Nos. 21303153, 21273192, and 61204009), Program for Science & Technology Innovation Talents in Universities of Henan Province (14HASTIT008), and the Research Project of Basic and Advanced Technology of Henan Province (Grant No. 112300410106) for support. Z. Zheng is thankful for the support from Innovation Scientists and Technicians Troop Construction Projects of Henan Province (Grant No. 144200510014). H.-K. Kim is thankful for support from the Korean Government Scholarship Program. This work was supported by a regulatory science grant under the FDA Nanotechnology CORES Program and by the Office of Cosmetics and Colors, CFSAN/FDA (W.H., W.G.W., and J.-J.Y.). This Article is not an official U.S. FDA guidance or policy statement. No official support or endorsement by the U.S. FDA is intended or should be inferred.

REFERENCES

(1) Hoffmann, M. R.; Martin, S. T.; Choi, W.; Bahnemann, D. W. Environmental Applications of Semiconductor Photocatalysis. *Chem. Rev.* **1995**, *95*, 69−96.

(2) Chen, C. C.; Ma, W. H.; Zhao, J. C. Semiconductor-Mediated Photodegradation of Pollutants under Visible-Light Irradiation. *Chem. Soc. Rev.* **2010**, *39*, 4206−4219.

(3) Andreescu, S.; Ornatska, M.; Erlichman, J. S.; Estevez, A.; Leiter, J. C. *Biomedical Applications of Metal Oxide Nanoparticles, Fine Particles in Medicine and Pharmacy*; Matijević, E., Eds.; Springer: New York, 2012; Chapter 3, pp 57−100.

(4) Azam, A.; Ahmed, A. S.; Oves, M.; Khan, M. S.; Habib, S. S.; Memic, A. Antimicrobial Activity of Metal Oxide Nanoparticles against Gram-positive and Gram-negative Bacteria: A Comparative Study. *Int. J. Nanomed.* **2012**, *7*, 6003−6009.

(5) Zhang, X.; Qin, J.; Xue, Y.; Yu, P.; Zhang, B.; Wang, L.; Liu, R. Effect of Aspect Ratio and Surface Defects on the Photocatalytic Activity of ZnO Nanorods. *Sci. Rep.* **2014**, *4*, 4596.

(6) Mclaren, A.; Valdes-Solis, T.; Li, G.; Tsang, S. C. Shape and Size Effects of ZnO Nanocrystals on Photocatalytic Activity. *J. Am. Chem. Soc.* **2009**, *131*, 12540−12541.

(7) Tachikawa, T.; Yamashita, S.; Majima, T. Evidence for Crystal-Face-Dependent TiO_2 Photocatalysis from Single-Molecule Imaging and Kinetic Analysis. *J. Am. Chem. Soc.* **2011**, *133*, 7197−7204.

(8) Li, Y.; Zhang, W.; Niu, J.; Chen, Y. Mechanism of Photogenerated Reactive Oxygen Species and Correlation with the Antibacterial Properties of Engineered Metal-Oxide Nanoparticles. *ACS Nano* **2012**, *6*, 5164−5173.

(9) Ullah, R.; Dutta, J. Photocatalytic Degradation of Organic Dyes with Manganese-Doped ZnO Nanoparticles. *J. Hazard. Mater.* **2008**, *156*, 194−200.

(10) Bian, Z.; Tachikawa, T.; Kim, W.; Choi, W.; Majima, T. Superior Electron Transport and Photocatalytic Abilities of Metal-Nanoparticle-Loaded TiO_2 Superstructures. *J. Phys. Chem. C* **2012**, *116*, 25444−25453.

(11) Su, R.; Tiruvalam, R.; He, Q.; Dimitratos, N.; Kesavan, L.; Hammond, C.; Lopez-Sanchez, J. A.; Bechstein, R.; Kiely, C. J.; Hutchings, G. J.; Besenbacher, F. Promotion of Phenol Photodecomposition over TiO_2 Using Au, Pd, and Au-Pd Nanoparticles. *ACS Nano* **2012**, *6*, 6284−6292.

(12) He, W. W.; Kim, H. K.; Wamer, W. G.; Melka, D.; Callahan, J. H.; Yin, J. J. Photogenerated Charge Carriers and Reactive Oxygen

Species in ZnO/Au Hybrid Nanostructures with Enhanced Photocatalytic and Antibacterial Activity. *J. Am. Chem. Soc.* **2014**, *136*, 750−757.
(13) He, W. W.; Zhou, Y. T.; Wamer, W. G.; Boudreau, M. D.; Yin, J. J. Mechanisms of the pH Dependent Generation of Hydroxyl Radicals and Oxygen Induced by Ag Nanoparticles. *Biomaterials* **2012**, *33*, 7547−7555.
(14) He, W. W.; Zhou, Y. T.; Wamer, W. G.; Hu, X.; Wu, X.; Zheng, Z.; Boudreau, M. D.; Yin, J. J. Intrinsic Catalytic Activity of Au Nanoparticles with Respect to Hydrogen Peroxide Decomposition and Superoxide Scavenging. *Biomaterials* **2013**, *34*, 765−773.
(15) He, W. W.; Liu, Y. T.; Wamer; Yin, J. J. Electron Spin Resonance Spectroscopy for the Study of Nanomaterial-mediated Generation of Reactive Oxygen Species. *J. Food Drug Anal.* **2014**, *22*, 49−63.
(16) Zhang, H.; Pokhrel, S.; Ji, Z.; Meng, H.; Wang, X.; Lin, S.; Chang, C. H.; Li, L.; Liu, R.; Li, R.; Sun, B.; Wang, M.; Liao, Y.; Xia, T.; Mädler, L.; Nel, A. E. PdO-Doping Tunes Bandgap Energy Levels as well as Oxidative Stress Responses to a p-Type Semiconductor Co_3O_4 In Vitro and In Vivo. *J. Am. Chem. Soc.* **2014**, *136*, 6406−6420.
(17) Lowry, O. H.; Rosebrough, N. J.; Farr, A. L.; Randall, R. J. Protein Measurement with the Folin Phenol Reagent. *J. Biol. Chem.* **1951**, *193*, 265−275.
(18) Gilbert, B.; Fakra, S. C.; Xia, T.; Pokhrel, S.; Mädler, L.; Nel, A. E. The Fate of ZnO Nanoparticles Administered to Human Bronchial Epithelial Cells. *ACS Nano* **2012**, *6*, 4921−4930.
(19) Zhang, L.; Jiang, Y.; Ding, Y.; Daskalakis, N.; Jeuken, L.; Povey, M.; O'Neill, A. J.; York, D. W. Mechanistic Investigation into Antibacterial Behaviour of Suspensions of ZnO Nanoparticles against *E. coli*. *J. Nanopart. Res.* **2010**, *12*, 1625−1636.
(20) van Aerle, R.; Lange, A.; Moorhouse, A.; Paszkiewicz, K.; Ball, K.; Johnston, B. D.; de-Bastos, E.; Booth, T.; Tyler, C. R.; Santos, E. M. Molecular Mechanisms of Toxicity of Silver Nanoparticles in Zebrafish Embryos. *Environ. Sci. Technol.* **2013**, *47*, 8005−8014.
(21) Adams, C. P.; Walker, K. A.; Obare, S. O.; Docherty, K. M. Size-Dependent Antimicrobial Effects of Novel Palladium Nanoparticles. *PLoS One* **2014**, *9*, No. e85981.
(22) Wilkinson, K. E.; Palmberg, L.; Witasp, E.; Kupczyk, M.; Feliu, N.; Gerde, P.; Seisenbaeva, G. A.; Fadeel, B.; Dahlen, S. E.; Kessler, V. G. Solution-Engineered Palladium Nanoparticles: Model for Health Effect Studies of Automotive Particulate Pollution. *ACS Nano* **2011**, *5*, 5312−5324.
(23) Yusop, R. M.; Unciti-Broceta, A.; Johansson, E. M. V.; Sánchez-Martín, R. M.; Bradley, M. Palladium-Mediated Intracellular Chemistry. *Nat. Chem.* **2011**, *3*, 239−243.
(24) Wang, C. C.; Wang, S.; Xia, Q.; He, W. W.; Yin, J. J.; Fu, P. P.; Li, J. H. Phototoxicity of Zinc Oxide Nanoparticles in HaCaT Keratinocytes-Generation of Oxidative DNA Damage During UVA and Visible Light Irradiation. *J. Nanosci. Nanotechnol.* **2013**, *13*, 3880−3888.
(25) Yin, J. J.; Liu, J.; Ehrenshaft, M.; Roberts, J. E.; Fu, P. P.; Mason, R. P.; Zhao, B. Phototoxicity of Nano Titanium Dioxides in HaCaT Keratinocytes-Generation of Reactive Oxygen Species and Cell Damage. *Toxicol. Appl. Pharmacol.* **2012**, *263*, 81.
(26) He, W. W.; Zhao, H. X.; Jia, H. M.; Yin, J. J.; Zheng, Z. Determination of Reactive Oxygen Species from ZnO Micro-Nano Structures with Shape-Dependent Photocatalytic Activity. *Mater. Res. Bull.* **2014**, *53*, 246−250.
(27) Zhao, H. T.; Joseph, J.; Zhang, H.; Karoui, H.; Kalyanaraman, B. Synthesis and Biochemical Applications of a Solid Cyclic Nitrone Spin Trap: A Relatively Superior Trap for Detecting Superoxide Anions and Glutathiyl Radicals. *Free Radical Biol. Med.* **2001**, *3*, 599−606.
(28) Tanaka, A.; Sakaguchi, S.; Hashimoto, K.; Kominami, H. Preparation of Au/TiO_2 with Metal Cocatalysts Exhibiting Strong Surface Plasmon Resonance Effective for Photoinduced Hydrogen Formation under Irradiation of Visible Light. *ACS Catal.* **2013**, *3*, 79−85.
(29) Zhang, Z.; Yates, J. T. Band Bending in Semiconductors: Chemical and Physical Consequences at Surfaces and Interfaces. *Chem. Rev.* **2012**, *112*, 5520−5551.
(30) Yan, F.; Wang, Y.; Zhang, J.; Lin, Z.; Zheng, J.; Huang, F. Schottky or Ohmic Metal−Semiconductor Contact: Influence on Photocatalytic Efficiency of Ag/ZnO and Pt/ZnO Model Systems. *ChemSusChem* **2014**, *7*, 101−104.